J Supercond Nov Magn (2018) 31:1315–1321
DOI 10.1007/s10948-017-4355-3

ORIGINAL PAPER

Study of $(DNPs)_x$/CuTl-1223 Nanoparticle-Superconductor Composites

M. Mumtaz[1] · Zafar Iqbal[2] · M. Raza Hussain[2] · Liaqat Ali[1] · M. Waqee-ur-Rehman[1] · M. Saqib[2]

Received: 3 September 2017 / Accepted: 13 September 2017 / Published online: 20 September 2017

Abstract Sol-gel and solid-state reaction methods were used to synthesize diamond nanoparticles (DNPs) and $(DNPs)_x$/CuTl-1223 ($x = 0$, 0.25, 0.50, and 1.00 wt.%) nanoparticle-superconductor composites, respectively. Effects of these DNPs on structural, morphological, compositional, and transport properties of CuTl-1223 superconducting phase were investigated by different experimental techniques such as X-ray diffraction (XRD), energy dispersive X-ray (EDX) spectroscopy, scanning electron microscopy (SEM), and resistivity versus temperature (R-T) measurements. The unchanged crystal structure and stoichiometry of host CuTl-1223 superconducting matrix with addition of DNPs gave evidence about the dispersion of nanoparticles at the grain boundaries of the host matrix, which may heal up the inter-granular voids and pores resulting in enhanced inter-grain connectivity. Critical transition temperature T_c (0) and hole concentration of CuTl-1223 superconductor were observed to be increased with addition of DNPs up to a certain optimum value (i.e. $x = 0.5$ wt.%).

Keywords $(DNPs)_x$/CuTl-1223 nanoparticle-superconductor composites · Diamonds nanoparticles · Superconducting properties

✉ M. Mumtaz
mmumtaz75@yahoo.com

[1] Materials Research Laboratory, Department of Physics, Faculty of Basic and Applied Sciences (FBAS), International Islamic University (IIU), Islamabad 44000, Pakistan

[2] Department of Physics, Riphah International University, I-14 Islamabad, Pakistan

1 Introduction

High-pressure synthesis imposes limitations to the use of high-temperature superconductors (HTSCs) at commercial level. $Cu_{0.5}Tl_{0.5}Ba_2Ca_{n-1}Cu_nO_{2n+4-\delta}$ (CuTl-12(n–1)n); $n = 2, 3, 4, \ldots$ superconducting family is of great interest for researchers due to its easy synthesis both at ambient and high pressure. $(Cu_{0.5}Tl_{0.5})Ba_2Ca_2Cu_3O_{10-\delta}$(CuTl-1223) is the most attractive phase of CuTl-based superconducting family due to low anisotropy, high critical current density (J_c), and high critical transition temperature (T_c) [1–3]. The cuprate HTSCs are granular in nature and exhibit weak inter-grain connectivity, which limits their performance [4, 5]. Besides the demerits of inter-grain voids and pores present in cuprate superconductors, they have some merits also, just like these spaces serve as natural flux pinning centers when external magnetic field is applied. So, it is important to address the inter-gain weak linkages by keeping it in mind that improvement in inter-grain connectivity should not suppress the flux pinning ability of the superconducting matrix. One of the most effective methods in this regard is to embed nanoparticles at grain boundaries, which could enhance the grains connectivity and also act as effective artificial pinning centers [6–11].

Nanostructures of different materials such as diamond, SiC, SiO_2, and CNTs were added to $YBa_2Cu_3O_{7-\delta}$ cuprate superconductor, and their effects were investigated [12–15]. Critical current densities and pinning energies were enhanced with doping of different concentration of these nanostructures. Critical temperature was increased significantly with addition of CNTs while a small suppression was observed in case of carbon and SiC nanostructures. The effects of CNTs' addition in Bi-2223 and CuTl-1223 superconducting matrices were also explored [16, 17]. It was observed that superconducting volume fraction and cell

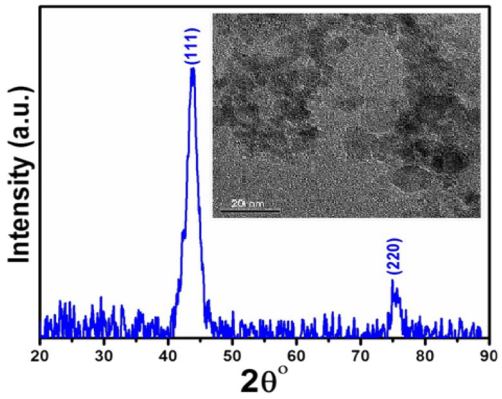

Fig. 1 XRD pattern of diamond nanoparticles. (In the *inset*, TEM image of diamond nanoparticles is shown)

parameters were remained un-altered by addition of these CNTs with small changes in grains size of host superconductors. CNTs' addition suppressed the superconducting transport properties of host matrices. The enhancement in critical current density, irreversible field (H_{irr}), and flux pinning ability of MgB_2 superconductor was observed with the doping of different concentrations of nanosized diamond [18]. The effect of carbon nanoparticles' addition on superconducting properties of MgB_2 superconductor was also investigated [19]. Lattice parameters and critical temperature were found to be decreased monotonically with increase in doping level of carbon nanoparticles, while the value of J_c was observed to be enhanced.

In the present research article, we are presenting the effect of DNPs addition in CuTl-1223 superconducting matrix. The added nanoparticles were embedded at inter-crystallite sites, which improved the inter-grain connectivity due to which superconducting transition temperature of host matrix was enhanced up to a certain optimum concentration level of these nanoadditives. The nanoparticles dispersed over inter-granular spaces may also improve the flux pinning ability of superconducting matrix, which is beneficial for high magnetic field applications of HTSCs.

2 Experimental Details

$(DNPs)_x$/CuTl-1223 nanoparticle-superconductor composites were synthesized by using two-step solid-state reaction method. Initially, the powders of Cu(CN), $Ca(NO_3)_2$, and $Ba(NO_3)_2$ were mixed in suitable ratios and ground in agate motor and pestle for 2 h. Then the mixed material was placed in quartz boats and fired in a pre-heated chamber furnace at 860 °C for 24 h followed by furnace cooling to room temperature. Same firing process was repeated with 1 h intermediate grinding. After second firing, thallium oxide (Tl_2O_3) and DNPs with different weight percent were mixed into the precursor material and ground again for 1 h in order to get homogenous mixture. The uniformly ground mixture was pelletized under 3.8 tons/cm^2 pressure and sintered at 860 °C for 10 min, enclosed in gold capsules. The sintered pellets were quenched to room temperature which yielded $(DNPs)_x$/CuTl-1223 nanoparticle-superconductor composites.

The electrical dc resistivity of bar-shaped 1.2 × 1.0 × 4.0 mm^3 samples were measured as a function of temperature (RT analysis) using four-probe technique. Phase purity and crystal structure of synthesized material were determined by XRD ($\lambda = 1.54056$ Å, X-ray source; CuKα) analysis. The surface morphology and elemental composition

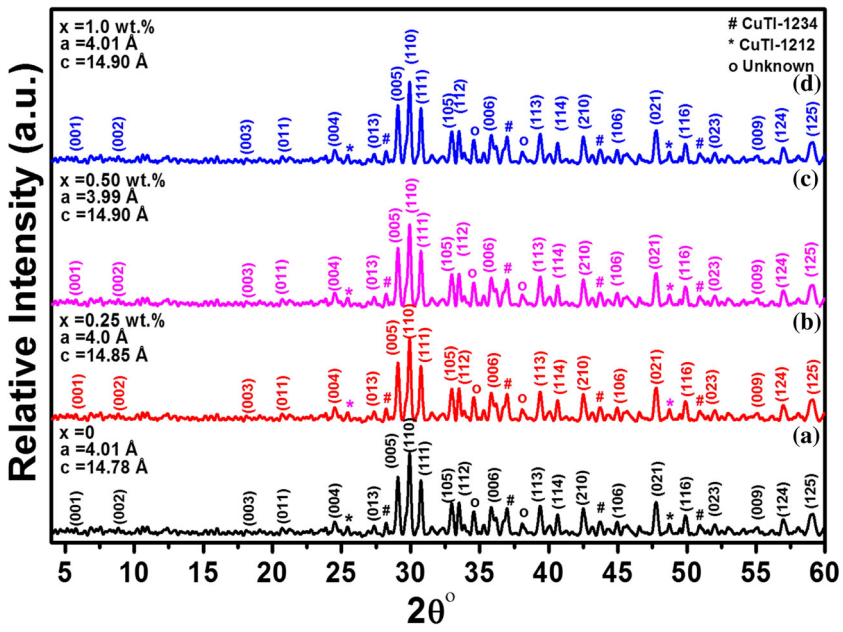

Fig. 2 XRD spectra of $(DNPs)_x$/CuTl-1223 nanoparticle-superconductor composites with $x = 0$, 0.25, 0.5, and 1.0 wt.%

of synthesized samples were determined by scanning electron microscopy (SEM) and energy dispersive X-ray (EDX) spectroscopy, respectively. To determine the mass density of samples, their mass and volume were measured. The mass and volume of each sample were measured by electronic balance with accuracy up to 0.001 g and by noting the increase in volume of water contained by calibrated test tube with insertion of sample inside water, respectively.

3 Results and Discussion

Figure 1 shows the XRD pattern of diamond nanoparticles which were added to CuTl-1223 superconducting matrix. The peaks of the pattern were indexed as (111) and (220) planes at $2\theta = 43.6°$ and 74.9°, respectively, which confirmed face-centered cubic structure of diamond nanoparticles [20]. The transmission electron microscopy (TEM) image of diamond nanoparticles is presented in the inset of Fig. 1. The average size of DNPs was 5 nm, which was determined from TEM micrograph.

Figure 2 shows XRD spectra of these composites with $x = 0$, 0.25, 0.50, and 1.00 wt.%. The most of the XRD peaks were well indexed according to the tetragonal structure of CuTl-1223 phase with P4/mmm symmetry. The cell parameters were determined using computer software named as check cell. XRD patterns revealed that crystal structure of host CuTl-1223 matrix does not change with the addition of diamond nanoparticles except small changes in lattice parameters. Unchanged crystal structure of host matrix with addition of nanoparticles shows that nanoparticles had not become the part of the unit cell of host matrix. So, in others words, it had been confirmed that nanoparticles occupied the inter-granular spaces and pores [21, 22]. Some un-indexed peaks of very small intensities were also observed in XRD spectra, which showed the existence of impurity and secondary phases like CuTl-1223, CuTl-1212, and CuTl-1234. Minimal change in lattice parameters may be attributed to stresses and strains generated by nanoparticles present at grain boundaries. Percentage volume fraction of different phases of superconductor was calculated by using equations as;

$$\text{CuTl-(1223)}\ \% = \frac{\sum I\,(1223)}{\sum\{I\,(1223) + I\,(1212) + I\,(1234) + I\,(Unknown)\}} \times 100\%$$

$$\text{CuTl-(1212)}\ \% = \frac{\sum I\,(1212)}{\sum\{I\,(1223) + I\,(1212) + I\,(1234) + I\,(Unknown)\}} \times 100\%$$

$$\text{CuTl-(1234)}\ \% = \frac{\sum I\,(1234)}{\sum\{I\,(1223) + I\,(1212) + I\,(1234) + I\,(Unknown)\}} \times 100\%$$

$$\text{CuTl-(unknown)}\ \% = \frac{\sum I\,(Unknown)}{\sum\{I\,(1223) + I\,(1212) + I\,(1234) + I\,(Unknown)\}} \times 100\%$$

where I(1223), I(1212), I(1234), and I(unknown) are intensities of phase CuTl-1223, CuTl-1212, CuTl-1224 and unknown peaks, respectively. Percentage volume fraction of different phases is shown in Table 1.

Figures 3 and 4 show the SEM and EDX micrographs of $(DNPs)_x$/CuTl-1223 ($x = 0$, 0.25, 0.5, and 1.0 wt.%) nanoparticle-superconductor composites. SEM images showed granular nature of synthesized composites. These micrographs show that the porosity in host superconducting matrix is reduced with increasing concentration of added nanoparticles, due to which inter-grain connectivity gets enhanced. SEM images also showed irregular and inhomogeneous distribution of diamond nanoparticles over inter-granular spaces of the composites. Similar results in SEM measurements were observed by some other research groups with inclusion of different nanostructures in cuprate

Table 1 The lattice parameters and percentage volume fraction of different phases of synthesized composites

(DNPs) nanoparticle contents (x%)	Tetragonal unit cell of CuTl-1223 phase a (Å)	Tetragonal unit cell of CuTl-1223 phase c (Å)	% Volume fraction of CuTl-1223 phase	% Volume fraction of CuTl-1212 phase	% Volume fraction of CuTl-1224 phase	% Volume fraction of unknown phase
$x = 0$	4.01	14.78	95.56	0.78	1.89	1.76
$x = 0.25$	4.0	14.85	94.76	0.95	2.17	2.12
$x = 0.5$	3.99	14.90	92.85	1.73	2.79	2.62
$x = 1.0$	4.01	14.90	93.94	1.23	2.57	2.25

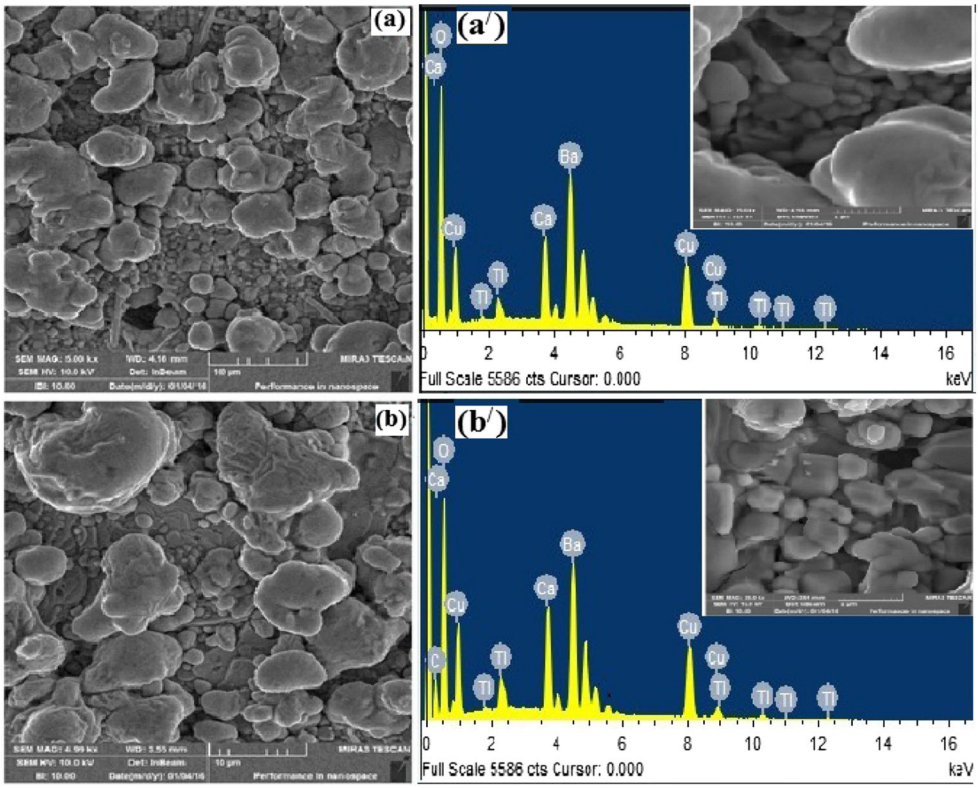

Fig. 3 $a, b, a^{/}, b^{/}$ The SEM and EDX spectra of $(DNPs)_x$/(CuTl-1223) nanoparticle-superconductor composites with $x = 0$ and 0.25 wt.%, respectively. (In the inset, SEM images at 2 μm scale are shown)

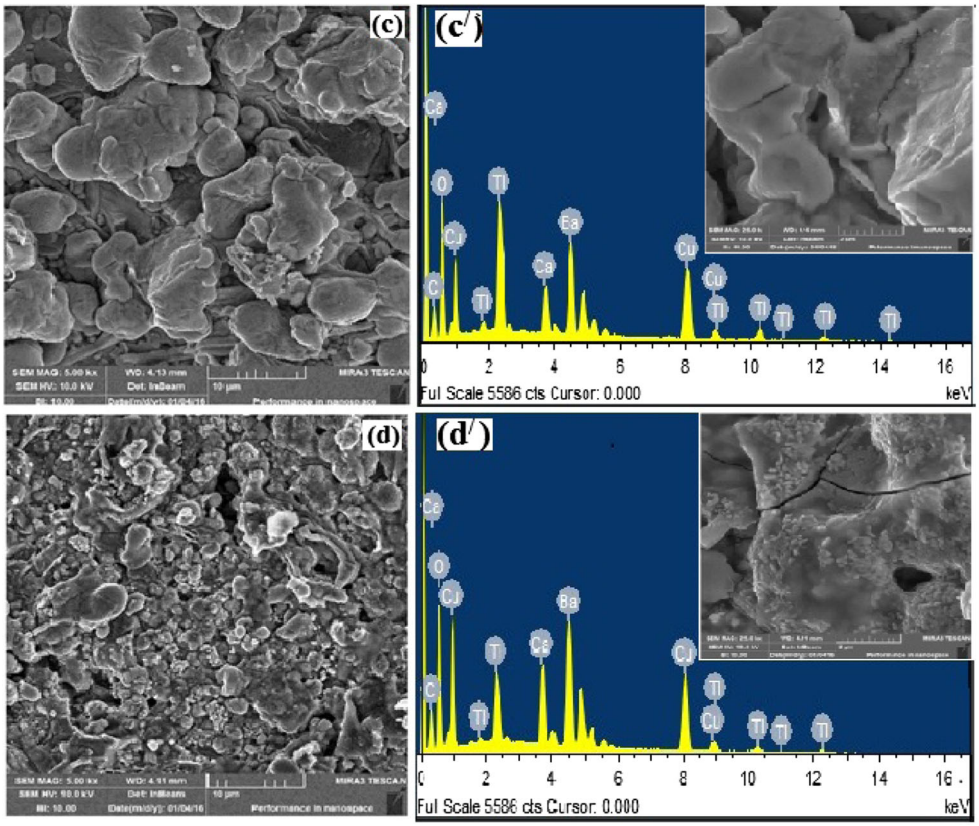

Fig. 4 $c, d, c^{/}, d^{/}$ The SEM and EDX spectra of $(DNPs)_x$/(CuTl-1223) nanoparticle-superconductor composites with $x = 0.5$ and 1.0 wt.%, respectively. (In the *inset*, SEM images at 2 μm scale are shown)

Table 2 Elemental analysis by EDX of $(DNPs)_x$/CuTl-1223 composites with $x = 0$, 0.25, 0.5, and 1 wt.%

Elements	$x = 0$			$x = 0.25$ wt.%			$x = 0.5$ wt.%			$x = 1.0$ wt.%		
	KeV	Mass%	Atom%	KeV	Mass%	Atom%	KeV	Mass%	Atom%	KeV	Mass%	Atom%
O K	0.535	27.61	54.97	0.535	25.39	54.42	0.535	26.09	52.42	0.540	19.92	45.72
Ca K	3.695	8.87	9.94	3.695	9.26	10.78	3.695	7.61	8.54	3.702	8.98	9.93
Cu L	0.952	24.36	26.27	0.952	25.41	24.88	0.952	25.63	28.08	0.960	29.98	20.32
Ba L	4.484	35.70	8.28	4.484	34.30	8.45	4.488	33.88	8.93	4.492	23.12	19.12
Tl M	2.325	3.46	0.54	2.325	5.36	0.82	2.318	6.04	0.95	2.315	16.95	2.76
C K	–	–	–	0.25	0.28	0.65	0.25	0.52	1.08	0.25	1.05	2.15
Total		100	100		100	100		100	100		100	100

superconductors [23, 24]. The mass and atom weight percent of different elements present in $(DNPs)_x$/CuTl-1223 ($x = 0$, 0.25, 0.5, and 1.0 wt.%) nanoparticle-superconductor composites were determined from EDX analysis of composites and tabulated in Table 2. The successful inclusion of DNPs is prominent from the entries of the table.

RT measurements of $(DNPs)_x$/CuTl-1223 ($x = 0$, 0.25, 0.5, and 1.0 wt.%) nanoparticle-superconductor composites in temperature range of 75 to 260 K is shown in Fig. 5. Figure 6 shows the variation in T_c (0) and T_c (onset) versus nanoparticles' concentration (x). Zero resistivity transition temperature (T_c (0)) of host CuTl-1223 superconducting matrix was observed to be enhanced monotonically up to certain optimum level of nanoparticles' concentration, i.e., $x = 0.5$ wt.% followed by suppression. The enhancement in T_c (0) can be attributed to the improvement in inter-grains connectivity by dispersion of nanoparticles at grain boundaries. The suppression in T_c (0) at $x = 1$ wt.% may be due to the high number density of nanoparticles at inter-granular spaces due to which scattering of charge carries takes place which results in cooper pairs breaking [25, 26]. Onset transition temperature (T_c (onset)) of host superconducting matrix was observed to be decreased with the addition of DNPs, which may be attributed to the enhanced rate of pairs breaking as compared with pairs formation due to scattering across nanoparticles [27]. The holes concentration in superconducting material can be found by Persland's equation [28, 29];

$$P = 0.16 - ((1 - T_c/T_c^{max})/82.6)^{1/2}$$

T_c^{max} is highest critical temperature of concerned superconducting family, which is 132 K in case of CuTl-1223 phase. The calculated values of holes concentration, mass density and ΔT_c (T_c (onset) $-T_c$ (0)) of $(DNPs)_x$/CuTl-1223; $x = 0$, 0.25, 0.50, and 1.0 wt.%) nanoparticle-superconductor

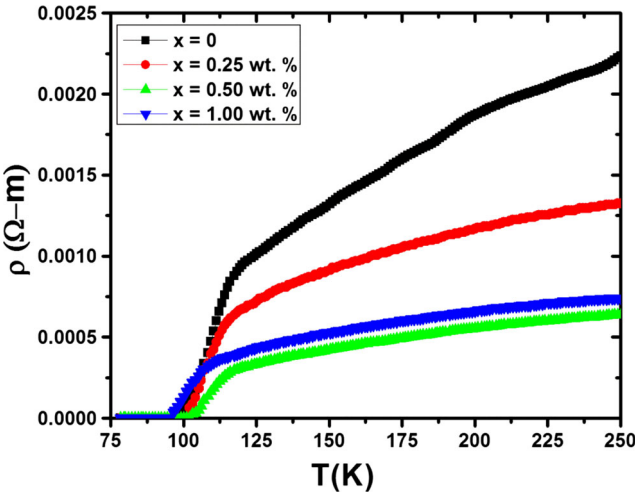

Fig. 5 Resistivity versus temperature measurements of $(DNPs)_x$/CuTl-1223 nanoparticle-superconductor composites with $x = 0$, 0.25. 0.5, and 1.0 wt.%

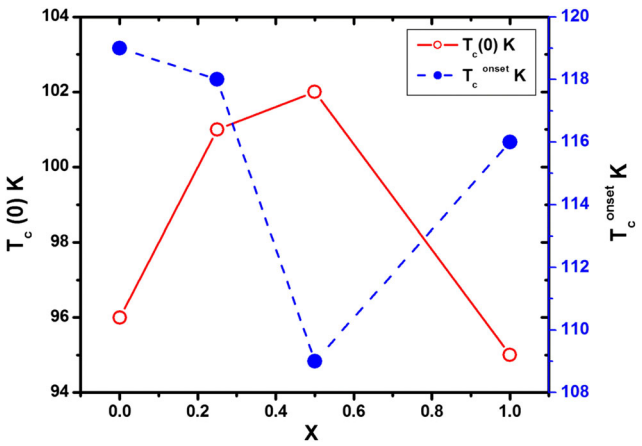

Fig. 6 Variation of critical temperatures (T_c (0) and T_c (onset)) versus $(DNPs)_x$/CuTl-1223 nanoparticle-superconductor composites with $x = 0$, 0.25. 0.5, and 1.0 wt.%

Table 3 Superconducting parameters and mass densities of $(DNPs)_x$/CuTl-1223 nanoparticle-superconductor composites with $x = 0$, 0.25, 0.5, and 1 wt.%

DNP nanoparticle contents	ΔT_c (K)	Hole concentrations	Mass density (g/cm^3)
0	23	0.1026	4.25
0.25 wt.%	17	0.1067	4.41
0.5 wt.%	07	0.1076	4.65
1.0 wt.%	21	0.1018	3.98

composites are tabulated in Table 3. Holes concentration was found to be increased by increasing concentration of DNPs, and it varied from 0.1018 to 0.1076. The highest hole concentration was observed for the $x = 0.5$ wt.% having a value of 0.1076, and this sample showed better superconducting characteristics in comparison with others.

4 Conclusion

$(DNPs)_x$/CuTl-1223 nanoparticle-superconductor composites were prepared with the help of the two-step solid-state reaction method. Tetragonal structure of CuTl-1223 superconducting phase remained unchanged after inclusion of DNPs, which indicated the dispersion of DNPs at grain boundaries. SEM micrographs of synthesized composites show the reduced porosity and enhancement inter-grain connectivity of host CuTl-1223 superconducting phase with the addition of DNPs. T_c (0) was increased with the addition of these nanoparticles of up to 0.5 wt.% followed by suppression. It can be concluded that addition of DNPs having suitable size and concentration may be helpful in improving the superconducting properties of cuprate high-temperature superconductors.

References

1. Ihara, H., Sekita, Y., Tateai, F., Khan, N.A., Ishida, K., Harashima, E., Kojima, T., Yamamoto, H., Tanaka, K., Tanaka, Y., Terada, N., Obara, H.: Superconducting properties of $Cu_{1-x}Tl_x$-1223 $[Cu_{1-x}Tl_x(Ba, Sr)_2Ca_2Cu_3O_{10-y}]$ thin films. IEEE Trans. Appl. Supercond. **9**, 1551 (1999)
2. Khan, N.A., Sekita, Y., Tateai, F., Kojima, T., Ishida, K., Terada, N., Ihara, H.: Preparation of biaxially oriented CuTl-1234 thin films. Physica C **320**, 39 (1999)
3. Khan, N.A., Khurram, A.A., Mazhar, M.: Effects of post-annealing on the infrared active phonon modes of low anisotropy (γ = 5-11) $Cu_{1-x}Tl_xBa_2Ca_2Cu_3O_{10-\delta}$ superconductor thin films. Physica C **407**, 23 (2004)
4. Ekin, J.W., Larson, T.M., Hermanm, A.M., Sheng, Z.Z., Togano, K., Kumakura, H.: Double-step behavior of critical current vs. magnetic field in Y-, Bi- and Tl-based bulk high-T_c superconductors. Physica C **160**, 489 (1989)
5. Passai, J., Lahtinen, M., Eriksson, J.T., Polak, M.: Experimental study of the intergranular magnetization of $(Bi, Pb)_2Sr_2Ca_2Cu_3O_{10+x}$ superconductors. Physica C **259**, 1 (1996)
6. Zhao, Y., Chen, C.H., Wang, J.S.: Flux pinning by NiO-induced nano-pinning centres in melt-textured YBCO superconductor. Supercond. Sci. Technol. **18**, S43 (2004)
7. Agranovski, I.E., Ilyushechkin, A.Y., Altman, I.S., Bostrom, T.E., Choi, M.: Methods of introduction of MgO nanoparticles into Bi-2212/Ag tapes. Physica C **434**, 115 (2006)
8. Farbod, M., Batvandi, M.R.: Doping effect of Ag nanoparticles on critical current of $YBa_2Cu_3O_{7-\delta}$ bulk superconductor. Physica C **471**, 112 (2011)
9. Patnaik, S., Gurevich, A., Bu, S.D., Kaushik, S.D., Choi, J., Eom, C.B., Larbalestier, D.C.: Thermally activated current transport in MgB_2 films. Phys. Rev. B **70**, 064503 (2004)
10. Azzouz, F.B., Zouaoui, M., Mellekh, A., Annabi, M., Tendeloo, G.V., Saleem, M.B.: Flux pinning by Al-based nanoparticles embedded in YBCO: a transmission electron microscopic study. Physica C **455**, 19 (2007)
11. Hamrita, A., Azzouz, F.B., Dachraoui, W., Saleem, M.B.: The effect of silver inclusion on superconducting properties of $YBa_2Cu_3O_y$ prepared using planetary ball milling. J. Supercond. Nov. Magn. **26**, 879 (2013)
12. Dadras, S., Ghavamipour, M.: Investigation of the properties of carbon-base nanostructures doped $YBa_2Cu_3O_{7-\delta}$ high temperature superconductor. Physica B **484**, 13 (2016)
13. Ma, Z., Liu, Y., Hu, W., Gao, Z., Yua, L., Dong, Z.: The enhancement of J_c in nano SiC-doped MgB_2 superconductors rapidly synthesized by activated sintering at low-temperature. Script. Mater. **61**, 836 (2009)
14. Mudgel, M., Awanaa, V.P.S., Kishana, H., Bhalla, G.L.: Significant improvement of flux pinning and irreversibility field in nano-carbon-doped MgB_2 superconductor. Solid State Commun. **146**, 330 (2008)
15. Rahul, S., Varghese, N., Vinod, K., Devadas, K.M., Thomas, S., Anees, P., Chattopadhyay, M.K., Roy, S.B., Syamaprasad, U.: Combined addition of nanodiamond and nano SiO2, an effective method to improve the in-field critical current density of MgB_2 superconductor. Mater. Res. Bull. **46**, 2036 (2011)
16. Saoudel, A., Amira, A., Boudjadja, Y., Mahamdioua, N., Amirouche, L., Varilci, A., Altintas, S.P., Terzioglu, C.: Study of the thermo-magnetic fluctuations in carbon nano-tubes added Bi-2223 superconductors. Physica B **429**, 33 (2013)
17. Khan, N.A., Aziz, S.: Single and multi-walled carbon nanotubes doped $(Cu_{0.5}Tl_{0.5})Ba_2Ca_2Cu_3O_{10-\delta}$ superconductors. J. Alloys Compd. **538**, 183 (2012)
18. Cheng, C.H., Zhang, H., Zhao, Y., Feng, Y., Rui, X.F., Munroe, P., Zeng, H.M., Koshizuka, N., Murakami, M.: Doping effect of nano-diamond on superconductivity and flux pinning in MgB_2. Supercond. Sci. Technol. **16**, 1182 (2003)
19. Soltanian, S., Horvat, J., Wang, X.L., Munroe, P., Dou, S.X.: Effect of nano-carbon particle doping on the flux pinning properties of MgB_2 superconductor. Physica C **390**, 185 (2003)
20. Zou, Q., Wang, M.Z., Li, Y.G.: Analysis of the nanodiamond particle fabricated by detonation. J. Exp. Nanosci. **5**, 319 (2010)
21. Habanjar, K., Barakat, M.M.E., Awad, R.: Investigation of physical and mechanical properties of $(BaSnO3)_x$(Bi,Pb)-2223 composite. J. Phys. Conf. Ser. **869**, 012030 (2017)
22. Qasim, I., Waqee-ur-Rehman, M., Mumtaz, M., Nadeem, K.: Role of Co nanoparticles in CuTl-1223 superconductor. Ceram. Int. **42**, 1122 (2016)
23. Hafiz, M., Abd-Shukor, R.: Effects of nano-sized NiF_2 addition in $Bi_{1.4}Pb_{0.6}Sr_2Ca_2Cu_3O_{10+\delta}$ superconductor. Adv. Mater. Res. **895**, 87 (2014)

24. Mohammad, N.H., Abou-Aly, A.I., Awad, R., Ibrahim, I.H., Roumie, M., Rekaby, M.: Mechanical and electrical properties of $(Cu_{0.5}Tl_{0.5})$-1223 phase added with nano-Fe_2O_3. J. Low Temp. Phys. **172**, 234 (2013)
25. Zhang, J., Liu, F., Cheng, G., Shang, J., Liu, J., Cao, S., Liu, Z.: Electron structure and vacancy properties and Al-substitution dependence of the positron life time in Y:1:2:3 superconducting ceramics. Phy. Lett. A **201**, 70 (1195)
26. Feng, S.J., Ma, J., Zhou, H.D., Li, G., Shi, L., Liu, Y., Fang, J., Li, X.G.: Energy dissipation in $Bi_2Sr_2CaCu_2O_{8+\delta}$ single crystal. Physica C **386**, 22 (2003)
27. Wu, H.Y., Ruan, K.Q., Yin, J., Huang, S.L., Lv, Z.M., Li, M., Cao, L.Z.: Effect of K and Nd substitutions on superconductivity of Bi2223 superconductors. Supercond. Sci. Technol. **20**, 1189 (2007)
28. Zelati, A., Amirabadizadeh, A., Kompany, A., Salamati, H., Sonier, J.: Effects of Dy_2O_3 nanoparticle addition on structural and superconducting properties of BSCCO. Ind. J. Sci. Technol. **7**, 123 (2014)
29. Bilgili, O., Selamet, Y., Kocabas, K.: Effects of Li substitution in Bi-2223 superconductors. J. Supercond. Nov. Magn. **21**, 439 (2008)